

Phase diagram of a rapidly-rotating two-component Bose gas

E. Ö. Karabulut^{1,4}, F. Malet², G. M. Kavoulakis³, and S. M. Reimann¹

¹*Mathematical Physics, LTH, Lund University, P.O. Box 118, SE-22100 Lund, Sweden*

²*Department of Theoretical Chemistry and Amsterdam Center for Multiscale Modeling, FEW, Vrije Universiteit, De Boelelaan 1083, 1081HV Amsterdam, The Netherlands*

³*Technological Educational Institute of Crete, P.O. Box 1939, GR-71004, Heraklion, Greece*

⁴*Physics Department, Faculty of Science, Selcuk University, TR-42075, Konya, Turkey*

(Dated: June 29, 2018)

We derive analytically the phase diagram of a two-component Bose gas confined in an anharmonic potential, which becomes exact and universal in the limit of weak interactions and small anharmonicity of the trapping potential. The transitions between the different phases, which consist of vortex states of single and multiple quantization, are all continuous because of the addition of the second component.

PACS numbers: 03.75.Kk, 03.75.Lm, 05.30.Jp

One of the remarkable features of cold atomic gases is their high degree of tunability, allowing for a precise and flexible control over most of the experimental parameters, and paving the way for many different potential applications of these systems. On the experimental side, remarkable progress has been made by, e.g., the realization of confining potentials of various functional forms (see, e.g., [1, 2]), or by the creation of mixtures of different atomic species, see, e.g., [3].

Two-component rotating Bose-Einstein condensates have been investigated thoroughly for the case of harmonic confinement, [3]. One of the most interesting phenomena is the presence of so-called “coreless vortices” that occur when only one of the two components carries all the angular momentum and forms a vortex state around the second one, which remains at rest at the vortex core [3]. Indeed, the presence of the second, non-rotating component gives rise to an effective anharmonic potential acting on the rotating component, and therefore allows the formation of multiply-quantized vortex states [4, 5]. These multiply-quantized vortex states are not energetically favorable in a single-component system in the case of harmonic confinement.

The rotational properties of a single-component Bose-Einstein condensate in the presence of an anharmonic potential have been addressed previously, employing the Gross-Pitaevskii mean-field approach, or the method of exact diagonalization [6–17]. In the case of harmonic confinement the rotational frequency of the trap Ω is limited by the trap frequency ω because of the centrifugal force: as $\Omega \rightarrow \omega$ the system enters a highly-correlated regime [18–20], while for $\Omega > \omega$ the system is not bounded. On the other hand, in the case of anharmonic confinement the system is bounded for any value of Ω .

In this study we consider a mixture of two Bose-Einstein condensates, which are confined in an anharmonic potential [21]. We investigate the rotational properties of this system as a function of the rotational frequency of the trap and the coupling between the atoms.

As we show, in the limit of weak interactions and small anharmonicity of the confining potential one can derive the corresponding phase diagram analytically solving a quadratic algebraic equation. Remarkably the phase diagram is exact and universal in these limits.

Our paper is organized as follows. We first focus on the case of zero and sufficiently weak interatomic interactions, where the order parameters of the two species are multiply-quantized vortex states. The simplicity of these states then allows us to investigate their stability as the coupling constant between the atoms increases, deriving the phase diagram of the system as a function of the interaction strength and of the rotational frequency of the trap. We finally analyse and interpret our results physically and compare them with those of a single-component system, as the inclusion of a second component changes the corresponding phase diagram rather drastically.

Model.—We consider a mixture of two distinguishable bosonic atoms, labelled A and B with equal mass M , but with different number of atoms N_A and N_B . The system is confined in a two-dimensional anharmonic potential of the form

$$V(\rho) = \frac{1}{2}M\omega^2\rho^2[1 + \lambda(\frac{\rho}{a_0})^2], \quad (1)$$

where ρ is the radial coordinate in cylindrical coordinates, ω is the trap frequency, $a_0 = \sqrt{\hbar/(M\omega)}$ is the oscillator length, and λ is a positive dimensionless parameter measuring the strength of the anharmonicity of the trapping potential. Along the axial direction, the density is assumed to be homogeneous within a width Z , with a total density per unit length $\sigma = (N_A + N_B)/Z$. The intra- and inter-species interaction is modelled as a hard-core potential with scattering lengths for elastic atom-atom collisions a_{AA} , a_{BB} , and a_{AB} , which are assumed to be repulsive. The general formalism is given for any value of the scattering lengths, while the final results are presented for equal scattering lengths, $a_{AA} = a_{BB} = a_{AB} = a$. The dimensionless parameter σa thus gives the “strength” of the interatomic coupling.

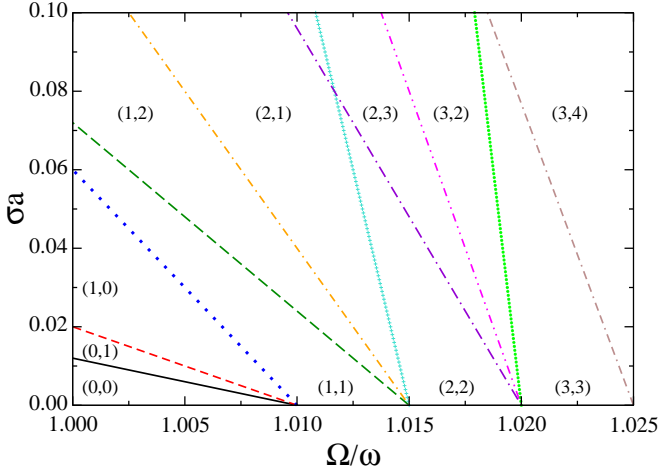


FIG. 1: (Colour online) Phase diagram, where the x axis is the frequency of rotation of the trap Ω/ω and the y axis is the coupling σa , for equal scattering lengths. The lines show the discontinuous transitions between the states $(m, n) \equiv (\Psi_A = \Phi_m; \Psi_B = \Phi_n)$. Here $\lambda = 0.005$ and $N_A/N_B = 2$.

Within the mean-field approximation the two order parameters Ψ_A and Ψ_B obey the following coupled nonlinear, Gross-Pitaevskii-like, differential equations, which in the rotating frame have the form

$$-\frac{\hbar^2 \nabla^2}{2M} \Psi_i + V(\rho) \Psi_i + (g_{ii} |\Psi_i|^2 + g_{ij} |\Psi_j|^2) \Psi_i - \Omega \hat{L}_z \Psi_i = \mu_i \Psi_i, \quad (2)$$

with $(i = A, B; j = B, A)$. Here \hat{L}_z is the axial component of the angular momentum operator, μ_i is the chemical potential of each component and $g_{ij} = 4\pi\hbar^2 \sigma a_{ij}/M$.

Discontinuous transitions.—Starting with the case of zero coupling, $\sigma a = 0$, and small anharmonicity, $\lambda \ll 1$, the order parameters Ψ_A and Ψ_B are given by the eigenstates of the harmonic potential with no radial nodes $\Phi_m(\rho, \phi) \propto \rho^m e^{im\phi} e^{-\rho^2/2a_0^2}$, where m is the quantum number that corresponds to the angular momentum $m\hbar$ (assumed to be positive). The single-particle energy spectrum E_m of the above states Φ_m scales quadratically with m , $E_m = \hbar\omega[1 + m + \lambda(m+1)(m+2)/2]$, as opposed to the harmonic potential, where $E_m \propto m$. As a result, as Ω increases, the system undergoes discontinuous phase transitions between the states Φ_m .

For weak coupling, $\sigma a \ll 1$, the effect of interactions may be treated perturbatively. The energy of the system in a state of (m, n) , where component A is in the state Φ_m , and component B is in the state Φ_n , is

$$\begin{aligned} \mathcal{E}_{m,n} = & x_A E_m + x_B E_n \\ & + \hbar\omega\sigma a \left(\alpha_{AA} x_A^2 \frac{(2m)!}{2^{2m}(m!)^2} + \alpha_{BB} x_B^2 \frac{(2n)!}{2^{2n}(n!)^2} \right. \\ & \left. + 2\alpha_{AB} x_A x_B \frac{(m+n)!}{2^{m+n}(m!n!)} \right). \end{aligned} \quad (3)$$

Here, $x_{A,B} = N_{A,B}/N$ and $\alpha_{ij} = a_{ij}/a$. The critical frequencies for transitions between different states of (m, n) can be calculated by comparing the energies in the rotating frame. Figure 1 shows the corresponding phase boundaries for a fixed population imbalance $N_A/N_B = 2$ and a weak anharmonicity, with $\lambda = 0.005$. In the absence of interactions the corresponding critical frequencies are degenerate. However, these degeneracies are lifted by the interactions, as seen in Fig. 1. For a fixed coupling and increasing Ω the system first undergoes a (discontinuous) transition to the state where the component with smaller number of atoms carries all the angular momentum and the other component remains static, which is a so-called coreless vortex state. Then, with increasing Ω , a vortex state forms in the larger component, while the smaller one becomes static. Finally, a vortex state forms in both components for a sufficiently large value of Ω . It is interesting that the same result is obtained in the case of mixtures in a purely harmonic potential [4, 5].

Continuous transitions.—As the interaction strength increases, the states of multiple quantization become unstable, as the energy of the system is minimized by mixing states of different angular momentum in the order parameters Ψ_A and Ψ_B . The multiply-quantized vortex states undergo continuous, second-order phase transitions. It turns out that the order parameters above the phase boundaries are of the form

$$\Psi_A = c_m \Phi_m + c_{m+q} \Phi_{m+q}, \quad \Psi_B = d_n \Phi_n + d_{n+q} \Phi_{n+q}. \quad (4)$$

Sufficiently close to the phase boundary, the coefficients c_m and d_n are of order unity, while the other two coefficients in Eq. (4) tend to zero. For this reason we keep in the energy only the terms which are up to quadratic in c_{m+q} and d_{n+q} ,

$$\begin{aligned} \mathcal{E} = & \frac{x_A}{S_A} (E_m c_m^2 + E_{m+q} c_{m+q}^2) + \frac{x_B}{S_B} (E_n d_n^2 + E_{n+q} d_{n+q}^2) \\ & + \frac{x_A^2}{S_A^2} (c_m^4 V_{m,m,m,m}^{AA} + 4c_m^2 c_{m+q}^2 V_{m,m,m,q,m,m+q}^{AA}) \\ & + \frac{x_B^2}{S_B^2} (d_n^4 V_{n,n,n,n}^{BB} + 4d_n^2 d_{n+q}^2 V_{n,n,n,q,n,n+q}^{BB}) \\ & + 2 \frac{x_A x_B}{S_A S_B} (c_m^2 d_n^2 V_{m,n,m,n}^{AB} + c_{m+q}^2 d_n^2 V_{m+q,n,m,n+q}^{AB} \\ & + d_{n+q}^2 c_m^2 V_{m,n+q,m,n+q}^{AB} + 2c_{m+q} d_{n+q} c_m d_n V_{n,m+q,n+q,m}^{AB}), \end{aligned} \quad (5)$$

where $S_A = c_m^2 + c_{m+q}^2$ and $S_B = d_n^2 + d_{n+q}^2$. Since the “pure” states $\Psi_A = \Phi_m$ and $\Psi_B = \Phi_n$ provide an extremum of the energy at the phase boundaries, the first-order derivatives of the energy in the rotating frame, $\mathcal{E}_{\text{rot}} = \mathcal{E} - (m+n)\hbar\Omega$, with respect to c_{m+q} and d_{n+q} vanish at the phase boundary. Therefore, the stability of the states of multiple quantization is determined by the eigenvalues of a two by two matrix whose elements

consist of the second-order derivatives of the energy with respect to c_{m+q} and d_{n+q} , i.e., $M_{1,1} = \partial^2 \mathcal{E}_{\text{rot}} / \partial c_{m+q}^2$, $M_{2,2} = \partial^2 \mathcal{E}_{\text{rot}} / \partial d_{n+q}^2$, and $M_{1,2} = \partial^2 \mathcal{E}_{\text{rot}} / \partial c_{m+q} \partial d_{n+q}$. The resulting matrix elements along the diagonal are

$$M_{1,1} = 2x_A(E_{m+q} - E_m - q\hbar\Omega) + 4x_A^2[2V_{m,m+q,m,m+q}^{AA} - V_{m,m,m,m}^{AA}] + 4x_A x_B[V_{m+q,n,m+q,n}^{AB} - V_{m,n,m,n}^{AB}], \quad (6)$$

$$M_{2,2} = 2x_B(E_{n+q} - E_n - q\hbar\Omega) + 4x_B^2[2V_{n,n+q,n,n+q}^{BB} - V_{n,n,n,n}^{BB}] + 4x_A x_B[V_{m,n+q,m,n+q}^{AB} - V_{m,n,m,n}^{AB}], \quad (7)$$

while the off-diagonal element is $M_{1,2} = 4x_A x_B V_{m,n+q,m+q,n}^{AB}$, where

$$V_{k,l,m,n}^{ij} = \hbar\omega\sigma a_{ij} \frac{(k+l)!}{2^{k+l}\sqrt{k!l!m!n!}} \delta_{k+l,m+n}. \quad (8)$$

When all the eigenvalues of this matrix are positive, the system is stable. However, as soon as any of the eigenvalues becomes negative, an instability occurs via a second-order and continuous phase transition. Assuming equal scattering lengths, we derive the following general expression for the phase boundaries of the ‘‘pure’’ states $\Psi_A = \Phi_m$ and $\Psi_B = \Phi_n$ for $n = m$, which is given by

$$(\sigma a)_q = \frac{1}{2} \frac{E_{m+q} - E_m - q\Omega}{V_{m,m,m,m} - V_{m,m+q,m,m+q}}. \quad (9)$$

The parameter q in the above expression can take any value, provided that $m + q \geq 0$.

The result of the calculation described above is shown in the phase diagram depicted in Fig. 2, which is the main result of this study. The phase boundaries corresponding to these continuous transitions (triangular regions) remain in between the straight lines of discontinuous phase transitions of absolute energetic stability shown in Fig. 1, which implies that the transitions between the phases of multiply quantized vortex states are no longer discontinuous. As long as the interaction strength has a non-zero value, they are continuous. The resulting phase diagram obtained for the two-component case in this respect is different from that of the one-component case for which the transitions between phases are found to be both continuous and discontinuous [13].

The part of the phase boundary which represents the instability towards the mixed states with $q = -1$ are vertical due to the fact that the denominator of Eq. (9) becomes zero (i.e., $V_{m,m,m,m} = V_{m,m-1,m,m-1}$) for this unstable mode. The lines corresponding to the unstable mode with $q = 1$ have negative slope, since

$$(\sigma a)_{q=1} = \frac{m+1}{V_{m,m,m,m}} [1 - \Omega + \lambda(m+2)]. \quad (10)$$

Thus, the region of stability takes the shape of a triangle for the pure state with $m = 1$. The lines with positive

slope cutting the other triangular regions in Fig. 2 denote the phase boundaries of the most unstable mode for the states with $m \geq 2$. Accordingly, when $m = 2$ and $m \geq 6$, we find that the most unstable mode corresponds to $q = -2$. For the intermediate phases with $m = 3, 4$, and 5 there is a transient regime where $q = -3$.

As the rotational frequency increases, we observe that the region of stability of the multiply-quantized vortex states extends further, up to the points where the lines with positive slope cut the triangular regions. For sufficiently large values of m , demanding that $(\sigma a)_{q=1} = (\sigma a)_{q=-2}$ and ignoring terms of order of $1/m$, we find that $\Omega \approx 1 + \lambda(m+1)$. In other words, for large m , the lines with positive slope cut the ones with negative slope right at the top of the triangle.

In the obtained phase diagram, we have determined triple points, where three phases coexist [10, 13]. As it is seen from Fig. 2, the states (2, 2), (3, 3), and (4, 4) have such triple points, where the two phase boundaries with positive and negative slopes intersect. For example, in the phase (2, 2) around the point where the two corresponding phase boundaries cut each other, there is a doubly-quantized vortex state, a doubly-quantized vortex state with a single vortex around it, and two-singly-quantized vortex states. In the fast-rotating regime, $\Omega > \omega$, the effective potential due to the confinement and the centrifugal potential has a ‘‘Mexican hat’’ form, which leads to a hole in the density of the cloud at the trap center. This hole appears first at (4, 4), as it is seen in Fig. 3, where we show schematic plots of the density and of the phase of the two order parameters Ψ_A and Ψ_B for the regions above the phases (2, 2), (3, 3), (4, 4), and (5, 5). The instability of the phase (3, 3) is towards (Φ_0, Φ_3) , which has a non-vanishing density at the center of the cloud. On the other hand, the instability of the state (4, 4) is towards (Φ_1, Φ_4) , which does vanish at the origin. Therefore, beyond the phase (3, 3) there is always a node in the density of the cloud at the center of the trap. From the plots in Fig. 3 we also see that the density minima of the one component coincide with the density maxima of the other component. The total density of the cloud thus remains as close as possible to axial symmetry along these phase boundaries.

The phase diagram that we have evaluated is exact and universal in the limit of weak interactions and weak anharmonicity of the trapping potential. In the single-component case the phase diagram is also universal, however it is only partly exact [13] because there are also discontinuous phase transitions, where the phase boundaries can only be evaluated approximately. On the other hand, in the present problem all the phase boundaries shown in Fig. 2 are continuous and thus are all exact. The phase diagram is universal in the sense that it is invariant under changes of the degree of anharmonicity λ of the trapping potential (provided that $\lambda \ll 1$), under proper rescaling of the two axes.

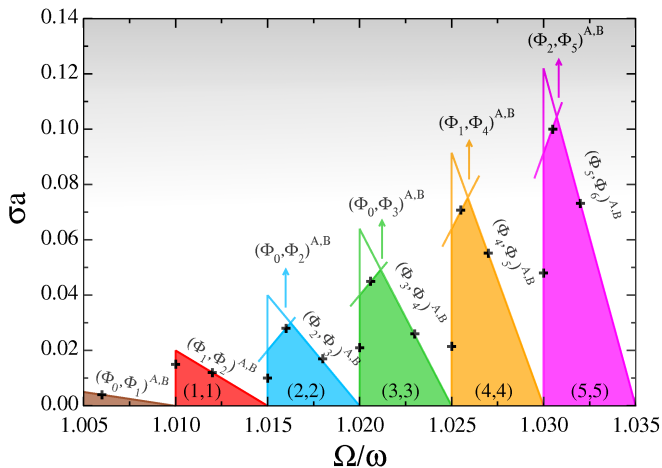


FIG. 2: (Colour online) Phase diagram, where the x axis is the frequency of rotation of the trap Ω/ω and the y axis is the coupling σa , for equal scattering lengths. All the lines show continuous transitions. Here $(m, m) \equiv (\Psi_A = \Phi_m; \Psi_B = \Phi_m)$, while $(\Phi_n, \Phi_m)^{A,B} \equiv (\Psi_A = c_n \Phi_n + c_m \Phi_m; \Psi_B = d_n \Phi_n + d_m \Phi_m)$ denotes the states of the form of Eq. (4). Here $\lambda = 0.005$ and $N_A/N_B = 2$.

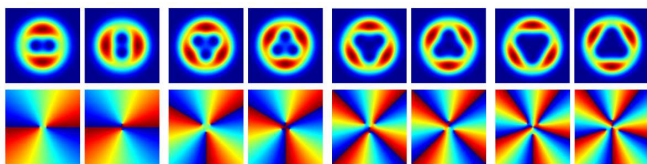


FIG. 3: (Color online) Density (upper) and phase (lower plots) of the component A (left) and B (right plots). These plots correspond to the “mixed” phases $(\Phi_0, \Phi_2)^{A,B}$, $(\Phi_0, \Phi_3)^{A,B}$, $(\Phi_1, \Phi_4)^{A,B}$, and $(\Phi_2, \Phi_5)^{A,B}$ from left to right.

Numerical results.—We have confirmed the phase boundaries shown in Fig. 2 numerically for various values of the coupling and of the rotational frequency. Since the transitions are continuous, we start from the phases of multiple quantization found in Fig. 1 for a fixed Ω and increase the coupling. We choose the initial state $\Psi_A = \Phi_n$, $\Psi_B = \Phi_m$ adding some more states with different angular momentum with very small amplitude and then propagate those in imaginary time using of a fourth-order split-step Fourier method [22]. Below the phase boundaries the amplitudes of the extra components decay, while above the boundary one of the small amplitudes increases, indicating the formation of a mixed state. The result of this calculation is shown as the crosses in the phase diagram of Fig. 2. The numerical results are in good agreement with the exact analytical solution. However, the discrepancy between the results of the two methods grows rapidly with increasing λ , since our analytical approach is perturbative.

Summary.—In summary, we have examined the phase diagram of a mixture of two Bose-Einstein condensed

gases confined in an anharmonic potential under rotation, as a function of the strength of the coupling constant and of the rotational frequency of the trap. We have shown that it is possible to derive the corresponding phase diagram analytically, reducing the problem to the evaluation of the roots of an algebraic equation of second degree. It is also remarkable that the presence of a second component makes the solution of this problem in a sense simpler than its one-component counterpart.

In the case of a single component, for sufficiently weak interactions the cloud undergoes discontinuous phase transitions between phases of multiple quantization. Here, while there are still phases of vortex states of multiple quantization, the transition between them takes place via continuous transitions. This becomes possible via vortex states which enter the two components successively from infinity, moving continuously towards the trap center.

The phase diagram we have evaluated is exact for sufficiently weak interactions and for small anharmonicity of the trapping potential. As long as these two assumptions are not violated, it is also universal. In the results of our study we have assumed equal scattering lengths for inter- and intra-species collisions. In the more general case, i.e., when they are not equal to each other (and/or the masses are unequal), the phase boundaries are no longer straight lines. However, the problem is still of the same level of difficulty. Given the simple and systematic behaviour of the evaluated phase diagram, it would be interesting to confirm these results experimentally.

We acknowledge discussions with A. D. Jackson. This work was financed by the Swedish Research Council and originated from a collaboration within the “POLATOM” Research Networking Programme of the European Science Foundation (ESF). E. Ö. K. is supported by the Turkish Council of Higher Education (YÖK) within the scope of the “Post-Doctoral Research Scholarship Programme”.

-
- [1] K. Henderson, C. Ryu, C. MacCormick, and M. G. Boshier, *New J. Phys.* **11**, 043030 (2009).
 - [2] Vincent Bretin, Sabine Stock, Yannick Seurin, and Jean Dalibard, *Phys. Rev. Lett.* **92**, 050403 (2004).
 - [3] K. Kasamatsu, M. Tsubota, and M. Ueda, *Int. J. Mod. Phys. B* **19**, 1835 (2005).
 - [4] S. Bargi, J. Christensson, G. M. Kavoulakis, and S. M. Reimann, *Phys. Rev. Lett.* **98**, 130403 (2007).
 - [5] J. Christensson, S. Bargi, K. Kärkkäinen, Y. Yu, G. M. Kavoulakis, M. Manninen, and S. M. Reimann, *New J. Phys.* **10**, 033029 (2008).
 - [6] A. L. Fetter, *Phys. Rev. A* **64**, 063608 (2001).
 - [7] E. Lundh, *Phys. Rev. A* **65**, 043604 (2002).
 - [8] K. Kasamatsu, M. Tsubota, and M. Ueda, *Phys. Rev. A* **66**, 053606 (2002).
 - [9] U. R. Fischer and G. Baym, *Phys. Rev. Lett.* **90**, 140402

- (2003).
- [10] G. M. Kavoulakis and G. Baym, *New J. Phys.* **5**, 51 (2003).
- [11] E. Lundh, A. Collin, and K.-A. Suominen, *Phys. Rev. Lett.* **92**, 070401 (2004).
- [12] A. Aftalion and I. Danaila, *Phys. Rev. A* **69**, 033608 (2004).
- [13] A. D. Jackson, G. M. Kavoulakis, and E. Lundh, *Phys. Rev. A* **69**, 053619 (2004).
- [14] A. D. Jackson and G. M. Kavoulakis, *Phys. Rev. A* **70**, 023601 (2004).
- [15] G. M. Kavoulakis, A. D. Jackson, and G. Baym, *Phys. Rev. A* **70**, 043603 (2004).
- [16] S. Bargi, G. M. Kavoulakis, and S. M. Reimann, *Phys. Rev. A* **73**, 033613 (2006).
- [17] M. Correggi, F. Pinsker, N. Rougerie, and J. Yngvason, *Phys. Rev. A* **84**, 053614 (2011).
- [18] N. R. Cooper, *Advances in Physics* **57**, 539 (2008).
- [19] A. L. Fetter, *Rev. Mod. Phys.* **81**, 647 (2009).
- [20] H. Saarikoski, S. M. Reimann, A. Harju, and M. Manninen, *Rev. Mod. Phys.* **82**, 2785 (2010).
- [21] C.-H. Hsueh, T.-L. Horng, S.-C. Gou, and W. C. Wu, *Phys. Rev. A* **84**, 023610 (2011).
- [22] S. A. Chin and E. Krotscheck, *Phys. Rev. E* **72**, 036705 (2005).